A climate sensitivity estimate using global average observations and an Earth System model with a dynamic 3D ocean

R. Tonkonojenkov *,[1], R. Sriver [1], M. Goes[2,3], N. M. Urban[4], H. D. Matthews[5], M. Haran[6] and K. Keller[1,7]

[1] Department of Geosciences, Penn State University, University Park, PA, USA

[2] Cooperative Institute for Marine and Atmospheric Studies, University of Miami, Miami, FL, USA

[3] Atlantic Oceanographic and Meteorological Laboratory, NOAA, Miami, FL, USA

[4] Program in Science, Technology, and Environmental Policy (STEP), Woodrow Wilson School of Public and International Affairs, Princeton University, Princeton, NJ, USA

[5] Department of Geography, Planning and Environment, Concordia University, Montreal, QC, Canada

[6] Department of Statistics, Penn State University, University Park, PA, USA

[7] Earth and Environmental Systems Institute, Penn State University, University Park, PA, USA.

*Corresponding author email: rzt2-wrk@psu.edu

Abstract. Current climate model projections are deeply uncertain. This uncertainty is partly driven by the uncertainty in key model parameters such as climate sensitivity (CS), vertical ocean diffusivity (K_v), and strength of anthropogenic sulfate aerosol forcing. Past studies estimating these parameters typically rely on intermediate complexity models with simplified ocean components, and thus neglect the likely important feedbacks through dynamic ocean circulation changes. We improve on these studies by using an Earth Model of Intermediate Complexity (EMIC) with a dynamic three-dimensional ocean to estimate these climate parameters.

We perform a perturbed physics analysis with the University of Victoria Earth System Climate Model (UVic ESCM), varying parameters that affect CS, ocean vertical diffusion (through changing background vertical ocean diffusivity, K_{bg}), and the effects of anthropogenic sulfate aerosols. We use a statistical emulator that interpolates the UVic model output to parameter settings where the model was not evaluated. We adopt a Bayesian approach to constrain the model output with instrumental surface temperature and ocean heat observations. We use a Markov chain Monte Carlo method to obtain a probability distribution function (pdf) of these parameters.

Our results for climate sensitivity are consistent with previous studies. The mode of the climate sensitivity pdf is 2.9 °C, with the corresponding 95% credible interval ranging from 1.8 to 4.9 °C. The CS pdf is sensitive to the assumptions about the priors, and to the effects of anthropogenic sulfate aerosols.

Our method can be used with more complex climate models where climate sensitivity is diagnosed rather than prescribed.

1. Introduction

Climate hindcasts and projections are strongly affected by two key climate model parameters: climate sensitivity (CS) and vertical ocean diffusivity. Meridional overturning circulation, global temperature, and ocean heat accumulation that produces thermosteric sea level rise are good examples of decision-relevant climate variables that depend on these parameters [*Goes et al.*, 2010; *Knutti et al.*, 2002]. Better characterization of the uncertainty in these parameters is thus critical for future climate prediction.

Climate sensitivity is defined as the equilibrium near-surface temperature response to a doubling of atmospheric CO_2. CS is a measure of climate feedbacks that amplify or dampen the direct response of near-surface temperature to radiative forcings [*Andronova et al.*, 2007]. Vertical ocean diffusivity (K_v) is a parameter that influences heat uptake by the ocean. K_v parametrizes mixing processes below the grid scale of climate models. For the same climate sensitivity, the atmosphere will reach the equilibrium temperature specified by CS more slowly at larger K_v values, due to higher heat flux into the deep ocean [*NAS*, 1979].

In order to estimate these parameters from climate models and observations, one needs to know past climate forcings. This is because assumptions about these forcings influence climate sensitivities that best simulate historical climate. For example, if indirect cooling effects by the aerosols are ignored in the models, then lower climate sensitivities are needed to match the observational record [*Knutti and Hegerl*, 2008]. The forcings due to aerosols are especially uncertain. A large part of this uncertainty is due to anthropogenic sulfate aerosols [*Forster et al.*, 2007].

Parameters controlling climate sensitivity, vertical diffusion in the ocean, and strength of anthropogenic sulfate aerosols are commonly estimated using model runs and observations [*Knutti et al.*, 2002, 2003; *Forest et al.*, 2002, 2006; *Drignei et al.*, 2008; *Tomassini et al.*, 2007; *Edwards et al.*, 2007; *Sanso and Forest*, 2009]. Typically, an ensemble of model runs is used where the key parameters are systematically varied. The outputs from these runs are then compared with the observations, and the posterior probability distribution functions (pdfs) for model parameters are derived.

A simpler methodology selects only the model runs that are consistent with the observations using a broad, heuristic approach [*Knutti et al.*, 2003]. In this framework all parameter combinations that pass the consistency criterion are assigned a uniform probability, while those that do not receive a zero probability. These probabilities are then used to construct the posterior pdfs.

A more theoretically grounded approach uses Bayesian statistics. This approach needs: (i) a model ensemble, (ii) observations, (iii) a statistical model that relates climate model output to the observations, and (iv) prior information about the model parameters (priors). Each of these components have a corresponding section in this paper. In this framework, each parameter combination is associated with a likelihood that depends on how well the corresponding model output matches the observations [*Tomassini et al.*, 2007; *Sanso and Forest*, 2009]. The likelihood, $L(Y|\Theta)$, describes the degree of belief that the physical observations Y came from a climate model and a statistical model (describing the properties of data-model residuals) with unknown parameters Θ. Once the statistical model is defined, the likelihood $L(Y|\Theta)$ can be calculated from the residuals between the model output and the observations. In the Bayesian framework, the posterior probability

of the unknown parameters given the observations is proportional to $L(Y|\Theta)$, and to the prior probability of the parameters:

$$p(\Theta|Y) \propto L(Y|\Theta) \times p(\Theta). \quad (1)$$

While the posterior probability $p(\Theta|Y)$ can be evaluated on a grid of parameter values, this can become computationally too expensive if the parameter space is multidimensional. In such cases Markov Chain Monte Carlo (MCMC) methods [*Metropolis et al.*, 1953; *Hastings*, 1970] can be used. The MCMC generates a sequence of parameter values (a Markov chain) which may be treated approximately as samples from the posterior distribution. Hence, virtually any property of the posterior distribution can be approximated by a corresponding sample property of this sequence.

Intermediate Complexity Earth System models are frequently used for this analysis [*Forest et al.*, 2002, 2006; *Knutti et al.*, 2003; *Tomassini et al.*, 2007; *Sanso and Forest*, 2009]. The appeal of these models is that they can be run at many parameter settings with relative ease. At the same time these models still represent many relevant physical processes. While such models can be run hundreds of times, many more runs at arbitrary parameter values are needed for the MCMC sampling. To approximate model output at an arbitrary parameter setting, emulators (statistical approximators of climate models) can be used [e.g., *Drignei et al.* [2008]]. The emulators draw on information about model outputs at known parameter settings to interpolate the output to any desired parameter setting.

We improve on previous studies by performing parameter estimation analysis using an Earth System model with a full 3D ocean. We constrain model runs with atmospheric sur-

face temperature and ocean heat content observations to present probability distribution functions for key model parameters controlling the processes described above: climate sensitivity CS, background vertical ocean diffusivity K_{bg}, and a scaling parameter for the effects of anthropogenic sulfate aerosols A_{sc}. The use of the full 3D ocean allows for better representation of the non-linear effects of K_{bg} on ocean dynamics and currents (e.g., on the Meridional Overturning Circulation), and thus can lead to better simulation of metrics used to calculate the likelihood (i. e. ocean heat uptake). We present posterior joint and marginal pdfs for the parameters, and explore the sensitivity of the results to prior assumptions.

2. Model Ensemble and the Model Emulator

2.1. Model Description

We use the University of Victoria Earth System Climate Model (UVic ESCM) [*Weaver et al.*, 2001] for our analysis. The atmospheric component is a one-layer energy-moisture balance model, with winds prescribed using the NCAR/NCEP climatology. The oceanic component is a 3D model MOM2 [*Pacanowski*, 1995]. Both the atmospheric and the oceanic components have horizontal resolution of 1.8° (lat) × 3.6° (lon). The ocean has 19 depth levels. The model also includes terrestrial vegetation and carbon cycle [*Cox*, 2001], oceanic biogeochemistry based on *Schmittner et al.* [2005], and thermodynamic sea ice. We use the modified 2.8 version of the model. Specifically, we use a newer solar forcing, and include anthropogenic sulfate, volcanic aerosol, and additional greenhouse gas forcings as in *Tonkonojenkov* [2010].

2.2. Model parameters

2.2.1. Climate Sensitivity (CS)

Climate sensitivity is defined as the equilibrium response of global average near-surface temperature to a doubling of atmospheric CO_2. Climate sensitivity is diagnosed parameter in the UVic ESCM. Following the approach of *Matthews and Caldeira* [2007] and *Zickfeld et al.* [2009], we vary CS through an additional feedback parameter f that perturbs local outgoing longwave radiation:

$$Q^*_{PLW} = Q_{PLW} + f(T_t - T_0). \quad (2)$$

Here T_o is temperature at equilibrium (i. e. at the start of the transient run), T_t is a temperature at time t, Q_{PLW} is the planetary outgoing longwave radiation as calculated in the standard 2.8 version of the model and Q^*_{PLW} represents the modified outgoing longwave radiation. All terms except f are functions of latitude and longitude.

We determine the relationship between f and CS using a small ensemble of CO_2 doubling experiments with varying f values at $K_{bg} = 0.1$ cm^2 s^{-1}. The runs continue for 2250 years to capture the equilibrium response of the model to CO_2. The CS is diagnosed as the average global temperature during the last 50 years of the runs minus the 50 year average prior to doubling. This mapping neglects potential dependency of CS on K_{bg} at the same value of f. We adopt a prior range for CS from 1.1 to 11.2 (Table 1).

2.2.2. Background Vertical Ocean Diffusivity (K_{bg})

The rate at which surface temperatures adjust to radiative forcings is controlled by the rate at which heat is absorbed by the ocean. The vertical mixing of heat in the ocean is parameterized in UVic ESCM by a vertical diffusivity parameter K_v, which has contributions from tidal and background diffusivities [*Schmittner et al.*, 2009]:

$$K_v = K_{tidal} + K_{bg}. \quad (3)$$

We vary the background diffusivity K_{bg}. As in *Schmittner et al.* [2009] and *Goes et al.* [2010], the model is modified to limit K_v to ≥ 1 cm^2 s^{-1} in the Southern Ocean below 500 m for better agreement with observations. Following *Goes et al.* [2010], we adopt the prior range for K_{bg} from 0.1 to 0.5 cm^{2}s^{-1} (Table 1).

2.2.3. Anthropogenic Aerosol Scaling Factor (A_{sc})

The strength of anthropogenic sulfate aerosol forcings is modulated via the scaling parameter (A_{sc}). Specifically, this parameter multiplies the original sulfate albedo map (representing direct effects of anthropogenic sulfates) to obtain total (direct + indirect) effects [*Tonkonojenkov*, 2010]. This formulation assumes a linear relationship between the direct and the indirect effects for a given A_{sc}. We use the prior range for A_{sc} from 0 to 3 (Table 1).

2.3. Hindcast Model Runs

We run an ensemble of UVic ESCM model runs where we systematically vary the three parameters over their prior ranges. Specifically, K_{bg} is varied on a uniform grid with values of (0.1, 0.2, 0.3, 0.4, 0.5) cm^{2}s^{-1}. We sample CS at (1.14, 1.64, 2.15, 2.62, 3.11, 3.98, 5.36, 6.51, 8.20, 11.2) °C. The values for A_{sc} include (0, 0.75, 1.5, 2.25, and 3). These values form a quasi-cubic grid (Figure 4).

The model is first spun up from observed data fields for 2,500 years with forcings set at year 1800 values. After this, the ocean and the land carbon cycles are coupled to the atmospheric CO_2 which is held fixed at the 1800 value of 283.7 ppm, and the

model is integrated for an additional 1000 years. The historical runs continue from year 1800 to present using historic radiative forcings. Volcanic aerosols, anthropogenic sulfate aerosols, changes in solar constant, and additional greenhouse gases such as CH_4, N_2O and CFCs, are implemented following *Goes et al.* [2010] and *Tonkonojenkov* [2010]. The atmospheric CO_2 concentration forcing is from *Etheridge et al.* [1998] and *Keeling et al.* [2004], complemented by the RCP8.5 scenario data after year 2002 [*Moss et al.*, 2010; *Riahi et al.*, 2007].

2.4. Gaussian Process Emulator

The MCMC sampling requires a large number of model runs (> 10000) at arbitrary parameter values. Since it is computationally infeasible to run UVic ESCM at that many parameter settings, we use a statistical emulator that can approximate the model outputs at any parameter value. We adopt Gaussian Process (GP) emulation. This technique has been previously used for the purpose of climate model approximation by *Bhat* [2010] and *Sanso and Forest* [2009]. We are comparing two of the model outputs with observations: atmospheric surface temperature and upper (0-700 m) ocean heat content. We emulate model output as a function of climate parameters separately for temperature and for ocean heat content. For each tracer, we develop separate emulators for each time step during the years for which the observations are available.

We define model output of tracer k at time t as $f_{t,k}(\theta)$ where θ is a vector of model parameters (K_{bg}, CS, A_{sc}). The $f_{t,k}(\theta)$ is only defined on a discrete set of parameter values where the model was run. The purpose of the emulator is to estimate a function $\tilde{f}_{t,k}(\theta)$ approximating model output on the continuous parameter ranges specified in Table 1. In the following discussion we will consider the emulator for atmospheric surface temperature

at time t_0. The emulators for all other times, and for the second tracer (ocean heat content) follow a similar statistical model. The indices t and k will thus be dropped from the rest of the emulator description.

The emulator is developed in linearly rescaled coordinates with transformed parameters $\theta' = (K'_{bg}, CS', A'_{sc})$ each taking on a range from zero to unity. The emulator approximates the climate model output as:

$$\tilde{f}(\theta') = P(\theta') + Z(\theta'), \tag{4}$$

where P is a quadratic polynomial in model parameters, and Z is a zero-mean Gaussian Process with an isotropic covariance function. Specifically, the covariance between model output at parameters θ'_i and θ'_j is modeled as $mC(i,j)$ where m is a scale multiplier and C is defined by:

$$C(i,j) = \exp \frac{-D_{ij}}{l}. \tag{5}$$

Here $D_{i,j}$ is the Euclidean distance between the two model parameter settings and l is a range parameter (fixed at 0.6). This formulation ensures that model output at nearby parameter settings is highly correlated (i. e. model output is a smooth function of the parameters). We assume a nugget variance of zero. In other words, the emulator is equal to model output at the points of the ensemble design grid. We estimate the polynomial parameters and m. The optimized parameters provide the Best Linear Unbiased Estimate (BLUE) of $\tilde{f}(\theta')$.

Emulators for differing times and variables have different P and m. Henceforth all the emulators for all time steps and both tracers will be collectively referred to as the 'emulator'.

The emulator was extensively tested using the leave one out cross validation analysis. The emulator was found to perform adequately well (e.g., Figure 1) during the times when the variability of model output across the parameter space is large.

3. Observations

We use two observational constraints. The first is global average atmospheric surface / ocean surface temperatures from the HadCRUT3 dataset of the Hadley Center [*Brohan et al.*, 2006]. These observations are defined as anomalies with respect to 1850-1899 period average. The observations cover time period from 1850 to 2006 (Figure 2).

The second constraint is global total ocean heat content in the 0-700 m layer [*Domingues et al.*, 2008]. These observations span the period from 1950 to 2003, and are calculated as anomalies with respect to the whole observation period (Figure 2).

4. Statistical Model and Markov Chain Monte Carlo

We use a Bayesian parameter estimation method similar to *Tonkonojenkov* [2010]. In order to be able to evaluate the likelihood of observations given the unknown parameters $L(Y|\Theta)$ we need a statistical model that defines the relationship between the model (and the emulator) output and the observations. We refer to the emulator output by $\tilde{f}_{t,k}(\theta)$ (for time t, tracer k, and parameter combination θ). The observations are denoted by $y_{t,k}$. We adopt the statistical model:

$$y_{t,k} = \tilde{f}_{t,k} + b_k + \epsilon_{t,k}. \quad (6)$$

Thus, the discrepancy between the model and observations is due to the time constant bias b_k and time-varying error $\epsilon_{t,k}$. $\epsilon_{t,k}$ results from (i) model structural error, (ii) natural climate variability, (iii) emulator error, and (iv) observational error. $\epsilon_{t,k}$ is modeled as an autoregressive process of order 1 (AR1) with unknown AR1 parameters σ_k^2 and ρ_k. σ_k^2 represents the variance of the AR(1) innovations while ρ_k represents the autocorrelation of lag1 (i. e. correlation of $\epsilon_{t,k}$ with $\epsilon_{t-1,k}$). We assume independence between the model-data residuals for different tracers.

We draw samples approximately from the joint posterior $p(\Theta|Y)$ using the MCMC algorithm and generate the posterior probability distribution of $\Theta = (K_{bg}, CS, A_{sc}, \sigma_T, \rho_T, b_T, \sigma_{OHC}, \rho_{OHC}, b_{OHC})$, where subscript T refers to temperature and OHC - to ocean heat content. Our MCMC prechains are 50,000 members long, while the final chain has 300,000 members. We test the chains for convergence using the MCMC standard errors from the consistent batch means procedure [*Flegal et al.*, 2008; *Jones et al.*, 2006], and by repeating the assimilation with different starting values of the parameters for the final chain. Neither of these checks suggest any issues with convergence. Hence, we are satisfied that our MCMC-based inference provides reasonable estimates of the posterior pdfs.

5. Priors

We run two assimilation experiments. In the base case experiment we use non-uniform priors for climate sensitivity and background vertical ocean diffusivity. We refer to this

experiment as NON-UNIF. The priors for this experiment are listed in Table 1 and plotted in Figure 3. For K_{bg} the prior is Lognormal (-1.55, 0.59) cm^2 s^{-1} [*Bhat*, 2010]. The climate sensitivity prior incorporates weak prior information derived from current mean climate and Last Glacial Maximum constraints. Specifically, we use a product of normal inverse Gaussian distributions (NIG) of $NIG(\alpha = 1.8, \delta = 2.3, \beta = 1.2, \mu = 1.7)$ and $NIG(\alpha = 1.9, \delta = 3.3, \beta = 1.0, \mu = 1.3)$. We choose these distributions for their empirical ability to simultaneously fit the lower, upper, and best estimates in *Knutti and Hegerl* [2008], not because we have any theoretical motivation for the NIG distribution. While the central tendencies of the two NIG pdfs are generally compatible with past studies, the distributions are not based on any specific pdf. The combined prior distribution for CS has a mean of 3.25 °C, and the 90% interval from 1.7 to 5.2 °C. We use uniform priors for A_{sc} and for all statistical parameters over the ranges specified in Table 1.

To explore the sensitivity of the results to priors, we run a second assimilation experiment, where all priors are uniform over the ranges shown in Table 1. We refer to this experiment as UNIF.

6. Results

6.1. Probabilistic Hindcasts

The probabilistic hindcasts capture the overall temporal structure of the observations (Figure 2). Specifically, the bias-corrected emulator is able to correctly represent the trend due to greenhouse warming (black line). We add an AR1 error process (representing model, observational, and emulator error, as well as the natural variability) to each bias-corrected emulator from the sub-sampled MCMC chain to produce the 95% credible intervals. Overall, the method produces a reasonable surprise index (e.g., 1.9% of

the ocean heat content and 5.7% of the temperature observations lie outside of the 95% hindcast range).

6.2. Parameter Estimates

Under the baseline assumptions of non-uniform priors, posterior pdfs for climate sensitivity and vertical ocean diffusivity are broadly consistent with previous studies. The mode of climate sensitivity pdf is 2.9 °C, with the 95% posterior credible interval from 1.8 °C to 4.9 °C (Table 2). These values are broadly consistent with the likely range of 2 to 4.5 °C, and the most likely value of 3 °C given by the IPCC [*Solomon et al.*, 2007]. The mode is similar to results from [*Knutti et al.*, 2003; *Forest et al.*, 2006] and slightly higher than in [*Tomassini et al.*, 2007].

For K_{bg}, we estimate a mode of 0.11 cm^2 s^{-1}, and a mean of 0.20 cm^2 s^{-1} (Table 2, Figure 3). The pdf for K_{bg} was reported to depend on the tracers used to constrain this parameter [*Schmittner et al.*, 2009]. The mode of the K_{bg} matches results of *Schmittner et al.* [2009] based on global vertical ocean profiles of CFC11, and of $\Delta^{14}C$, and is slightly lower than 0.15 cm^2 s^{-1} reported in [*Goes et al.*, 2010] based on profiles of three tracers.

The estimated aerosol scaling factor has the most likely value of 1.1. This is broadly consistent with the default assumptions on the aerosol effects in the UVic ESCM (which imply the value of 1). Estimation of A_{sc} should be interpreted with caution because A_{sc} is implicitly including effects due to neglected forcings that might have emission or concentrations patterns similar to the anthropogenic sulfates. To better constrain A_{sc} it will be necessary to include these neglected forcings. Or, one could interpret the value of A_{sc} as representing the combined effect of direct+indirect aerosols, as well other neglected forcings.

As in previous studies, the climate sensitivity pdf, and its upper tail in particular, are sensitive to the assumptions about the priors [*Forest et al.*, 2002, 2006; *Sanso and Forest*, 2009; *Tomassini et al.*, 2007] (Figure 3). For example, replacing the expert prior with the uniform moves the upper bound of the 95% credible interval for CS to 10.2 °C (Table 2), in agreement with the results from *Forest et al.* [2006]. For this uniform prior case, there is a considerable probability mass above the upper bound of the IPCC likely range of 4.5 °C (Figure 3), similar to previous studies (e.g., *Forest et al.* [2006]; *Knutti et al.* [2003]). High climate sensitivities become possible in this case because the flat prior assigns them high weight to begin with, while the constraint provided by the observations is relatively weak. This suggests that it is crucial to use independent prior information during CS estimation whenever possible.

In addition, in the UNIF experiment the posterior pdf of K_{bg} is bimodal (Figure 3). Multimodal pdfs for K_{bg} have been previously reported by *Forest et al.* [2002] and *Tomassini et al.* [2007]. It is, thus far, unclear which physical mechanisms are driving this bimodality.

Joint bivariate pdfs for parameter pairs exhibit a complex structure (Figure 4), similar to the results from from *Tomassini et al.* [2007]. There is no pronounced correlation between K_{bg} and CS; nor between A_{sc} and K_{bg}. In contrast, climate sensitivity is positively correlated with A_{sc}, meaning that for higher climate sensitivity, higher indirect aerosol effects (relative to the direct effects) are needed to explain historical climate change. This indicates that reducing uncertainty in A_{sc} will help reduce uncertainty in climate sensitivity. Ruling out high values of A_{sc} is especially important, because this is where climate sensitivity pdf appears to be most sensitive to A_{sc} (Figure 4).

When the uniform priors on K_{bg} and CS are used, higher aerosol scaling values become possible, even though the prior on A_{sc} is the same in both cases. Because A_{sc} and CS are correlated, higher aerosol scalings are necessary to counteract higher warming due to larger climate sensitivities in the uniform prior case to match the observations.

7. Caveats

There are several caveats that bear mentioning. The first set of caveats deals with the Earth System model. Our model does not include all forcings (such as, for example, tropospheric ozone [*Forster et al.*, 2007]). The emission patterns of some of excluded forcings might be similar to anthropogenic sulfates, thereby biasing the A_{sc} estimates. Including thus far neglected forcings is the subject of future research. Also, we only consider a subset of uncertain climate parameters. Our results would change if these additional uncertainties were considered. The model relies on a number of simplifications. The representation of open ocean mixing is highly parametrized and ignores, for example, effects of tropical cyclones [*Sriver et al.*, 2010]. Also, we approximate a complex relationship between the indirect and the direct sulfate aerosol effects by a linear scaling as in *Forest et al.* [2002]. We vary the longwave radiation feedbacks to change climate sensitivity. In reality, the uncertainty in shortwave radiative feedbacks also contributes to the CS uncertainty [*Bony et al.*, 2006].

The second set of caveats is concerned with observations. When a short instrumental record is used, the results of our method can be influenced by natural climate variability and by observational errors comprising the residuals between the model and observations [*Tonkonojenkov*, 2010]. Adding more observations can improve the parameter estimates, as is using spatially resolved information.

Finally, limitations of the parameter estimation method deserve mentioning. We use a simplified likelihood function that does not account for error heteroskedasticity. Incorporating a more comprehensive likelihood function that captures a cross-correlation between the residuals for different tracers is the subject of future research.

8. Conclusions

Using a Bayesian approach, we fuse UVic ESCM model with global observations to estimate background vertical ocean diffusivity (K_{bg}), climate sensitivity (CS), and the scaling parameter for the effects of anthropogenic sulfate aerosols (A_{sc}). To our knowledge, these are the first results obtained with a model that includes a full 3D representation of ocean dynamics. We use a Gaussian Process emulator to provide a fast surrogate for the climate model at arbitrary parameter combinations. Our method is computationally inexpensive and can be used with more complex climate models. The parameter estimates can be used to make climate projections using the UVic ESCM in future studies.

The mode for K_{bg} is similar to previous results obtained using oceanic tracers such as CFC11, temperature, and $\Delta^{14}C$ as constraints. The K_{bg} pdf is sensitive to the assumptions about the priors.

Our climate sensitivity estimates are consistent with previous studies. Specifically, the mode of climate sensitivity using informative priors is 2.9 °C, with the 95% credible interval from 1.8 °C to 4.9 °C. As in previous studies, the upper tail of the CS pdf is sensitive to priors. The CS pdf depends critically on A_{sc}, with much higher climate sensitivities likely at high values of A_{sc}. The agreement with previous studies gives more confidence to using simpler climate models in studies estimating climate sensitivity.

Acknowledgments. We thank Michael Eby and other UVic ESCM model developers for providing the model and for helpful discussions. Very productive and though-provoking discussions with David Pollard, Sham Bhat, Andreas Schmittner, and Chris Forest are gratefully acknowledged. This work would not have been possible without the contributions from scientists that compiled the datasets utilized in this study, and who helped to build and refine the UVic ESCM model. This work was partially supported by NSF and USGS, as well as by the Canadian Foundation for Climate and Atmospheric Sciences (CFCAS GR-7059). All errors, views, and opinions are solely that of the authors.

References

Andronova, N., M. Schlesinger, S. Dessai, M. Hulme, and B. Li (2007), The concept of climate sensitivity: history and development, in *Human-induced Climate Change: An Interdisciplinary Assessment*, edited by M. Schlesinger, H. Kheshgi, J. Smith, F. de la Chesnaye, J. M. Reilly, T. Wilson, and C. Kolstad, Cambridge University Press.

Bhat, K. G. (2010), Inference for complex computer models and large multivariate spatial data with applications to climate science, Ph.D. thesis, The Pennsylvania State University.

Bony, S., et al. (2006), How well do we understand and evaluate climate change feedback processes?, *Journal of Climate*, *19*(15), 3445–3482.

Brohan, P., J. J. Kennedy, I. Harris, S. F. B. Tett, and P. D. Jones (2006), Uncertainty estimates in regional and global observed temperature changes: A new data set from 1850, *J. Geophys. Res. [Atmos.]*, *111*(D12), doi:10.1029/2005JD006548.

Cox, P. (2001), Description of the "TRIFFID" Dynamic Global Vegetation Model, *Tech. rep.*, Hadley Center technical note 24, Hadley Centre, Met Office, Berks, UK.

Domingues, C. M., J. A. Church, N. J. White, P. J. Gleckler, S. E. Wijffels, P. M. Barker, and J. R. Dunn (2008), Improved estimates of upper-ocean warming and multi-decadal sea-level rise, *Nature*, *453*(7198), 1090–U6, doi:10.1038/nature07080.

Drignei, D., C. E. Forest, and D. Nychka (2008), Parameter estimation for computationally intensive nonlinear regression with an application to climate modeling, *Ann. Appl. Stat.*, *2*(4), 1217–1230, doi:10.1214/08-AOAS210.

Edwards, T. L., M. Crucifix, and S. P. Harrison (2007), Using the past to constrain the future: how the palaeorecord can improve estimates of global warming, *Prog. Phys. Geog.*, *31*(5), 481–500, doi:10.1177/0309133307083295.

Etheridge, D. M., L. P. Steele, R. L. Langenfelds, R. J. Francey, J.-M. Barnola, and V. I. Morgan (1998), Historical CO_2 records from the Law Dome DE08, DE08-2, and DSS ice cores, in *Trends: A Compendium of Data on Global Change*, Carbon Dioxide Information Analysis Center, Oak Ridge National Laboratory, U.S. Department of Energy, Oak Ridge, Tenn., U.S.A.

Flegal, J. M., M. Haran, and G. L. Jones (2008), Markov Chain Monte Carlo: Can we trust the third significant figure?, *Statistical Science*, *23*(2), 250–260.

Forest, C. E., P. H. Stone, A. P. Sokolov, M. R. Allen, and M. D. Webster (2002), Quantifying uncertainties in climate system properties with the use of recent climate observations, *Science*, *295*(5552), 113–117.

Forest, C. E., P. H. Stone, and A. P. Sokolov (2006), Estimated PDFs of climate system properties including natural and anthropogenic forcings, *Geophys. Res. Lett.*, *33*(1),

391 doi:10.1029/2005GL023977.

392 Forster, P., et al. (2007), Chapter 2: Changes in Atmospheric Constituents and in Ra-
393 diative Forcing, in *Climate Change 2007: The Physical Science Basis. Contribution of*
394 *Working Group I to the Fourth Assessment Report of the Intergovernmental Panel on*
395 *Climate Change*, edited by S. Solomon, D. Qin, M. Manning, Z. Chen, M. Marquis,
396 K. B. Averyt, M. Tignor, and H. L. Miller, Cambridge Univ. Press, Cambridge, United
397 Kingdom and New York, NY, USA.

398 Goes, M., N. M. Urban, R. Tonkonojenkov, M. Haran, A. Schmittner, and K. Keller
399 (2010), What is the skill of ocean tracers in reducing uncertainties about ocean diapycnal
400 mixing and projections of the Atlantic Meridional Overturning Circulation?, *J. Geophys.*
401 *Res.*, *115*, doi:10.1029/2010JC006407, C12006.

402 Hastings, W. K. (1970), Monte Carlo sampling methods using Markov chains and their
403 applications, *Biometrika*, *57*(1), 97–109.

404 Jones, G. L., M. Haran, B. S. Caffo, and R. Neath (2006), Fixed-width output analysis for
405 Markov chain Monte Carlo, *Journal of the American Statistical Association*, *101*(476),
406 1537–1547, doi:10.1198/016214506000000492.

407 Keeling, C. D., T. P. Whorf, and the Carbon Dioxide Research Group (2004), Atmospheric
408 CO_2 concentrations (ppmv) derived from in situ air samples collected at Mauna Loa
409 Observatory, Hawaii, Scripps Institution of Oceanography (SIO), University of Califor-
410 nia, La Jolla, California, USA. Retrieved from http://cdiac.esd.ornl.gov/ftp/maunaloa-
411 co2/maunaloa.co2.

412 Knutti, R., and G. C. Hegerl (2008), The equilibrium sensitivity of the Earth's tempera-
413 ture to radiation changes, *Nature Geosc.*, *1*(11), 735–743, doi:10.1038/ngeo337.

Knutti, R., T. F. Stocker, F. Joos, and G. K. Plattner (2002), Constraints on radiative forcing and future climate change from observations and climate model ensembles, *Nature*, *416*(6882), 719–723.

Knutti, R., T. F. Stocker, F. Joos, and G. K. Plattner (2003), Probabilistic climate change projections using neural networks, *Clim. Dyn.*, *21*(3-4), 257–272, doi:10.1007/s00382-003-0345-1.

Matthews, H. D., and K. Caldeira (2007), Transient climate-carbon simulations of planetary geoengineering, *Proc. Natl. Acad. Sci. U. S. A.*, *104*(24), 9949–9954, doi:10.1073/pnas.0700419104.

Metropolis, N., A. W. Rosenbluth, M. N. Rosenbluth, A. H. Teller, and E. Teller (1953), Equation of state calculations by fast computing machines, *J. Chem. Phys.*, *21*(6), 1087–1092.

Moss, R. H., et al. (2010), The next generation of scenarios for climate change research and assessment, *Nature*, *463*(7282), 747–756, doi:10.1038/nature08823.

NAS (1979), Carbon dioxide and climate: A scientific assessment, *Tech. rep.*, US National Academy of Sciences, Washington, DC.

Pacanowski, R. C. (1995), MOM 2 documentation: Users guide and reference manual, version 1.0., *Tech. Rep. 3*, GFDL Ocean Group, Geophysical Fluid Dynamics Laboratory, Princeton, New Jersey.

Riahi, K., A. Gruebler, and N. Nakicenovic (2007), Scenarios of long-term socio-economic and environmental development under climate stabilization, *Technological Forecasting and Social Change*, *74*(7), 887–935, doi:10.1016/j.techfore.2006.05.026.

436 Sanso, B., and C. Forest (2009), Statistical calibration of climate system properties, *J.*
437 *Royal Stat. Soc. Ser. C - App. Stat.*, *58*(Part 4), 485–503.

438 Schmittner, A., A. Oschlies, X. Giraud, M. Eby, and H. L. Simmons (2005), A global
439 model of the marine ecosystem for long-term simulations: Sensitivity to ocean mixing,
440 buoyancy forcing, particle sinking, and dissolved organic matter cycling, GB3004, *Global*
441 *Biogeochem. Cycles*, *19*(3), doi:10.1029/2004GB002283.

442 Schmittner, A., N. M. Urban, K. Keller, and H. D. Matthews (2009), Using tracer obser-
443 vations to reduce the uncertainty of ocean diapycnal mixing and climate-carbon cycle
444 projections, GB4009, *Global Biogeochem. Cycles*, *23*, doi:10.1029/2008GB003421.

445 Solomon, S., et al. (2007), Technical summary, in *Climate Change 2007: The Physical Sci-*
446 *ence Basis. Contribution of Working Group I to the Fourth Assessment Report of the*
447 *Intergovernmental Panel on Climate Change*, edited by S. Solomon, D. Qin, M. Man-
448 ning, Z. Chen, M. Marquis, K. B. Averyt, M. Tignor, and H. L. Miller, Cambridge
449 University Press, Cambridge, United Kingdom and New York, NY, USA.

450 Sriver, R. L., M. Goes, M. E. Mann, and K. Keller (2010), Climate response to tropical
451 cyclone-induced ocean mixing in an Earth system model of intermediate complexity,
452 *Journal of Geophysical Research - Oceans*, *115*.

453 Tomassini, L., P. Reichert, R. Knutti, T. F. Stocker, and M. E. Borsuk (2007), Robust
454 Bayesian uncertainty analysis of climate system properties using Markov chain Monte
455 Carlo methods, *J. Clim.*, *20*(7), 1239–1254, doi:10.1175/JCLI4064.1.

456 Tonkonojenkov, R. (2010), What is the skill of climate parameter estimation methods?
457 A case study with global observational constraints, Master's thesis, The Pennsylvania
458 State University.

Weaver, A. J., et al. (2001), The UVic Earth System Climate Model: Model description, climatology, and applications to past, present and future climates, *Atmos.-Ocean*, *39*(4), 361–428.

Zickfeld, K., M. Eby, H. D. Matthews, and A. J. Weaver (2009), Setting cumulative emissions targets to reduce the risk of dangerous climate change, *Proceedings of the National Academy of Sciences of the United States of America*, *106*(38), 16,129–16,134.

Figure Captions

Figure 1. Top row: scatterplot of the temperature anomaly (with respect to the 1850-2006 mean) emulator predictions vs. actual model output values for years 1870, 1940, and 2000. Specifically, each of the parameter combinations of the ensemble was taken out one at a time, and the emulator was trained on the remaining 249 ensemble members. Then the emulator was used to predict the missing value. The 1:1 line is also shown. Bottom row: same for the ocean heat content anomalies (with respect to the 1950-2003 mean), for years 1960, 1980, and 2000. The emulator performance, of course, will be different for other times not shown here.

Figure 2. Probabilistic model hindcasts (grey shaded area), best fit model output (black line), and corresponding observations (red crosses) for the NON-UNIF assimilation experiment: (a) global average atmospheric surface temperature anomaly with respect to 1850-1899 mean [K] with corresponding observations of above surface / ocean surface temperatures from the HadCRUT3 dataset [*Brohan et al.*, 2006]; (b) upper ocean (0-700m) heat content anomaly with respect to 1950-2003 mean [1E22J], and observations from *Domingues et al.* [2008]. The grey area denotes the 95% credible intervals for model output taken from a 1000-member subsampled MCMC chain, with corresponding bias terms and AR1 error processes added. For the AR1 process simulations, the σ and ρ parameters were taken from the corresponding chain member. For the best fit model output, the maximum posterior probability model output was combined with the corresponding bias term.

Figure 3. Posterior pdfs (top row) and cdfs (bottom row) for model parameters obtained using both temperature and ocean heat content observations. Red: for the NON-UNIF experiment; blue: for the UNIF experiment. The dashed probability distribution lines represent the priors

used in the NON-UNIF experiment. The dashed whiskers in the box-and-whisker plots extend to the most extreme data point which is no more than 1.5 interquartile ranges from the box.

Figure 4. Bivariate joint pdfs for model parameters. Left: for the NON-UNIF experiment, right: for the UNIF experiment. The contour lines delineate the 90% and 95% posterior credible intervals. A 1000-member thinned MCMC chain is plotted using red dots. Parameters used for the UVic ESCM ensemble are shown in thick black circles.

Table 1: Prior ranges for the parameters used in the NON-UNIF experiment. Subscript T refers to the temperature data, and OHC refers to the ocean heat content data.

Parameter	Units	Lower Bound	Upper Bound	Prior Form
K_{bg}	$cm^2\ s^{-1}$	0.1	0.5	Lognormal(-1.55, 0.59)
CS	°C per CO_2 doubling	1.1	11.2	$NIG(\alpha = 1.8, \delta = 2.3, \beta = 1.2, \mu = 1.7) \times NIG(\alpha = 1.9, \delta = 3.3, \beta = 1.0, \mu = 1.3)$
A_{sc}	unitless	0	3	uniform
σ_T	°C	0.01	inf	uniform
σ_{OHC}	1×10^{22} J	0.01	inf	uniform
ρ_T	unitless	0.01	0.99	uniform
ρ_{OHC}	unitless	0.01	0.99	uniform
b_T	°C	-0.51	0.50	uniform
b_{OHC}	1×10^{22} J	-7	7	uniform

Table 2: Properties of the posterior pdfs of climate model parameters.

Parameter	Experiment	Mode	Mean	95% credible interval
K_{bg}	NON-UNIF	0.11	0.20	[0.10, 0.47]
	UNIF	0.49	0.30	[0.10, 0.50]
CS	NON-UNIF	2.9	3.1	[1.8, 4.9]
	UNIF	2.9	4.8	[1.7, 10.2]
A_{sc}	NON-UNIF	1.1	1.0	[0.35, 1.5]
	UNIF	1.4	1.2	[0.34, 1.8]
σ_T	NON-UNIF	0.10	0.10	[0.091, 0.11]
	UNIF	0.10	0.10	[0.091, 0.11]
σ_{OHC}	NON-UNIF	2.6	2.7	[2.2, 3.3]
	UNIF	2.6	2.7	[2.2, 3.4]
ρ_T	NON-UNIF	0.58	0.58	[0.44, 0.72]
	UNIF	0.58	0.58	[0.45, 0.72]
ρ_{OHC}	NON-UNIF	0.11	0.19	[0.019, 0.47]
	UNIF	0.13	0.19	[0.019, 0.47]
b_T	NON-UNIF	-0.032	-0.031	[-0.080, 0.020]
	UNIF	-0.035	-0.034	[-0.085, 0.018]
b_{OHC}	NON-UNIF	8.2×10^{-4}	-0.028	[-1.0, 0.90]
	UNIF	-0.017	-0.044	[-1.0, 0.88]

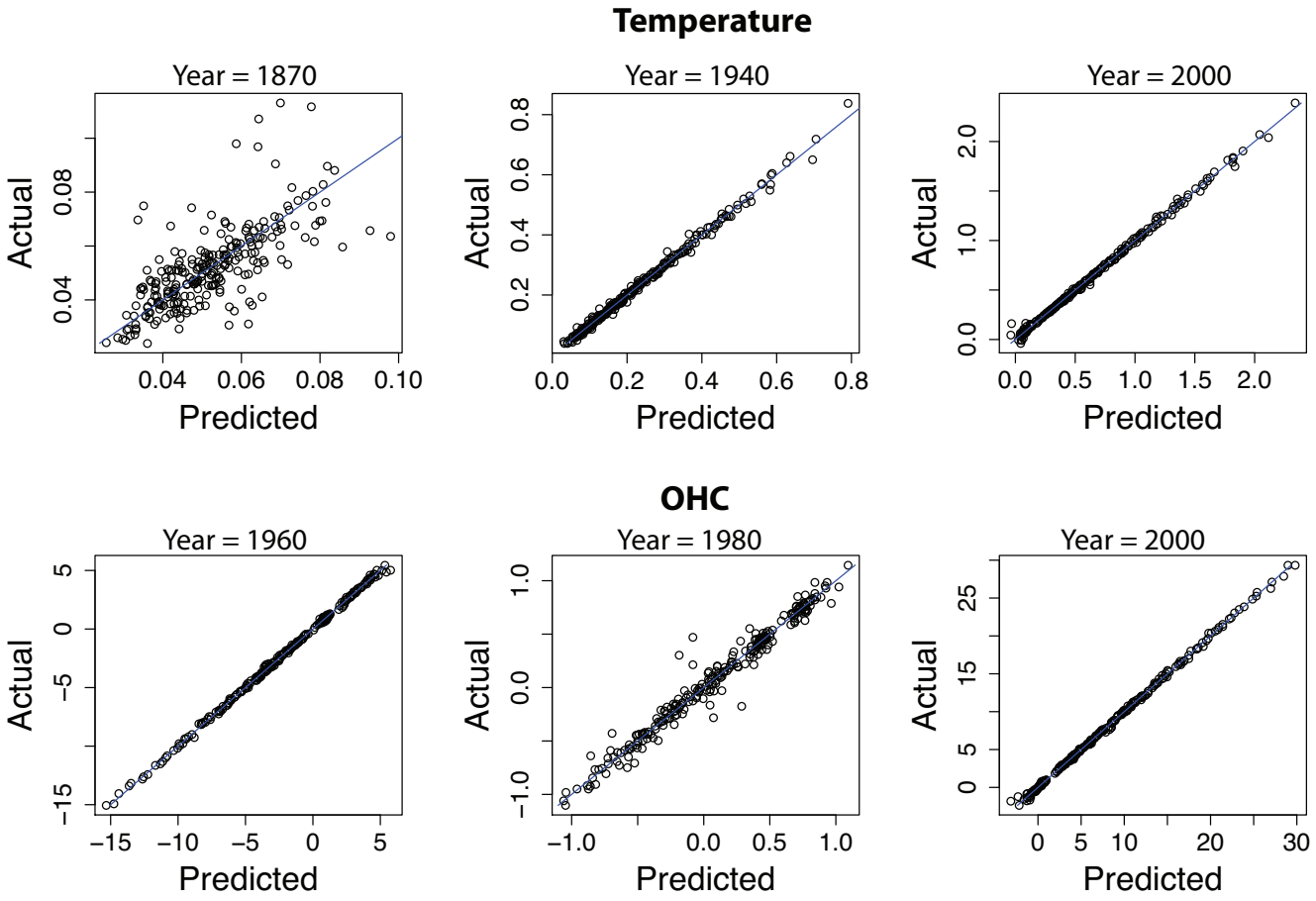

Figure 1: Top row: scatterplot of the temperature anomaly (with respect to the 1850-2006 mean) emulator predictions vs. actual model output values for years 1870, 1940, and 2000. Specifically, each of the parameter combinations of the ensemble was taken out one at a time, and the emulator was trained on the remaining 249 ensemble members. Then the emulator was used to predict the missing value. The 1:1 line is also shown. Bottom row: same for the ocean heat content anomalies (with respect to the 1950-2003 mean), for years 1960, 1980, and 2000. The emulator performance, of course, will be different for other times not shown here.

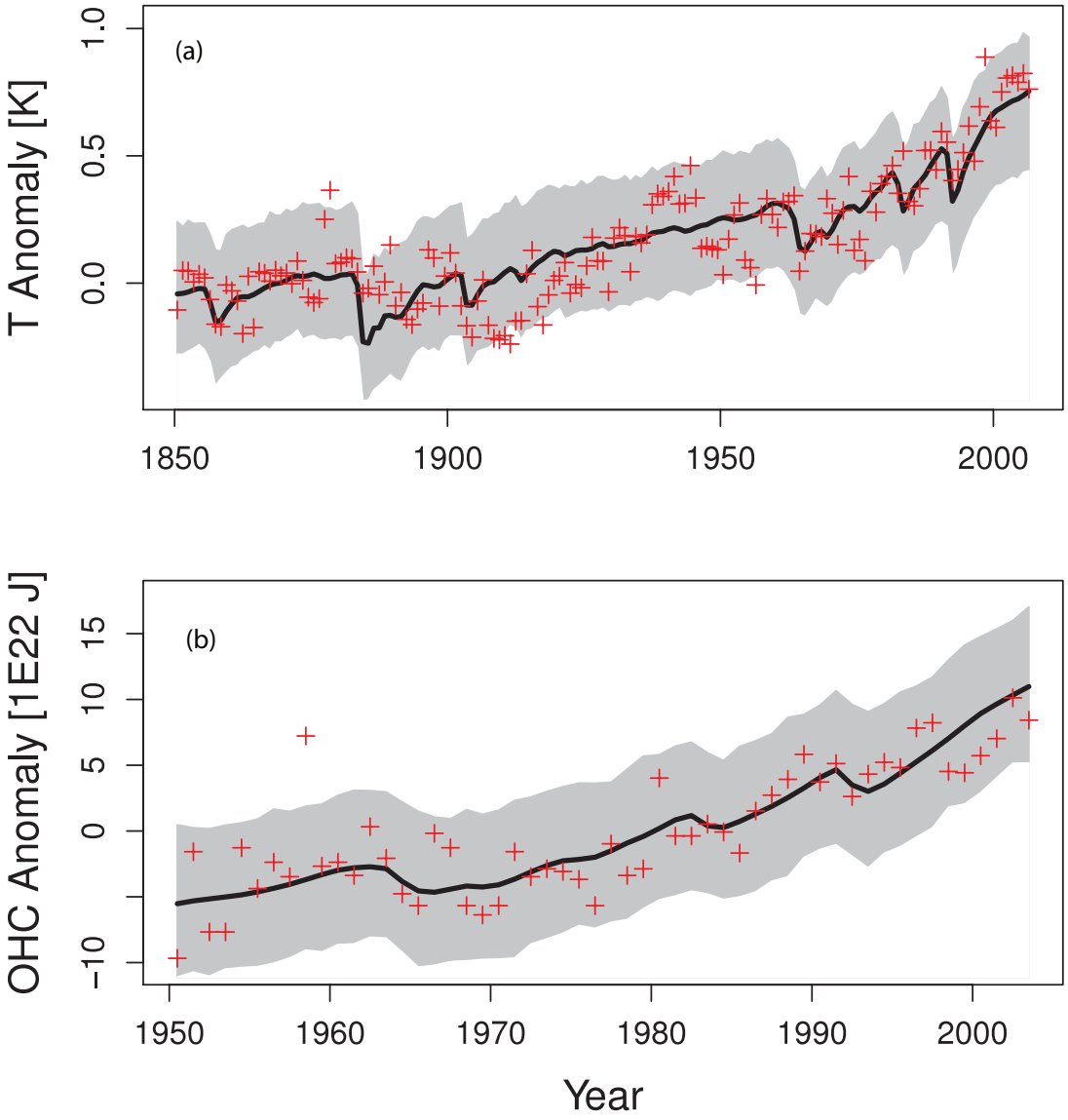

Figure 2: Probabilistic model hindcasts (grey shaded area), best fit model output (black line), and corresponding observations (red crosses) for the NON-UNIF assimilation experiment: (a) global average atmospheric surface temperature anomaly with respect to 1850-1899 mean [K] with corresponding observations of above surface / ocean surface temperatures from the HadCRUT3 dataset [*Brohan et al.*, 2006]; (b) upper ocean (0-700m) heat content anomaly with respect to 1950-2003 mean [1E22J], and observations from *Domingues et al.* [2008]. The grey area denotes the 95% credible intervals for model output taken from a 1000-member subsampled MCMC chain, with corresponding bias terms and AR1 error processes added. For the AR1 process simulations, the σ and ρ parameters were taken from the corresponding chain member. For the best fit model output, the maximum posterior probability model output was combined with the corresponding bias term.

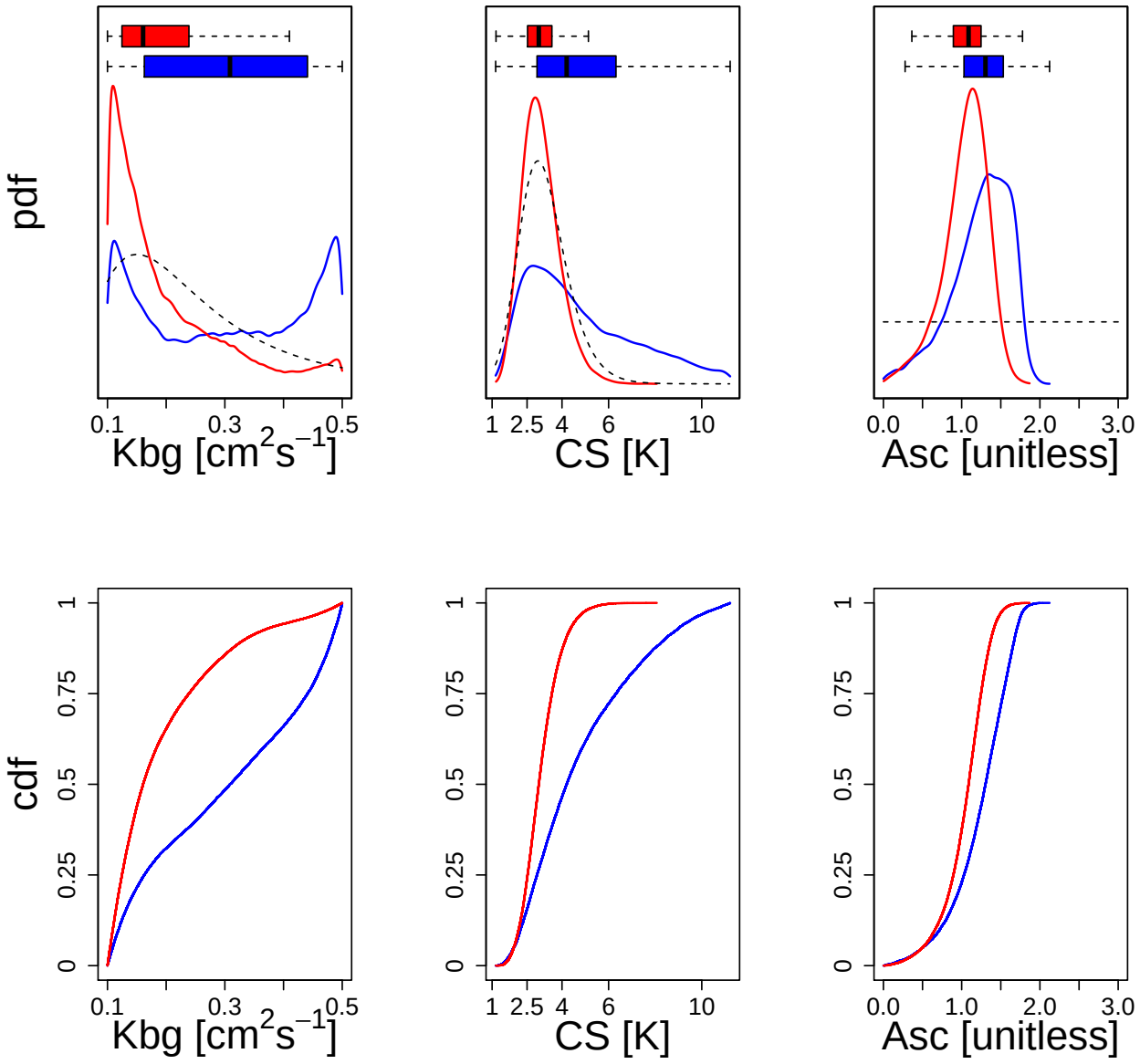

Figure 3: Posterior pdfs (top row) and cdfs (bottom row) for model parameters obtained using both temperature and ocean heat content observations. Red: for the NON-UNIF experiment; blue: for the UNIF experiment. The dashed probability distribution lines represent the priors used in the NON-UNIF experiment. The dashed whiskers in the box-and-whisker plots extend to the most extreme data point which is no more than 1.5 interquartile ranges from the box.

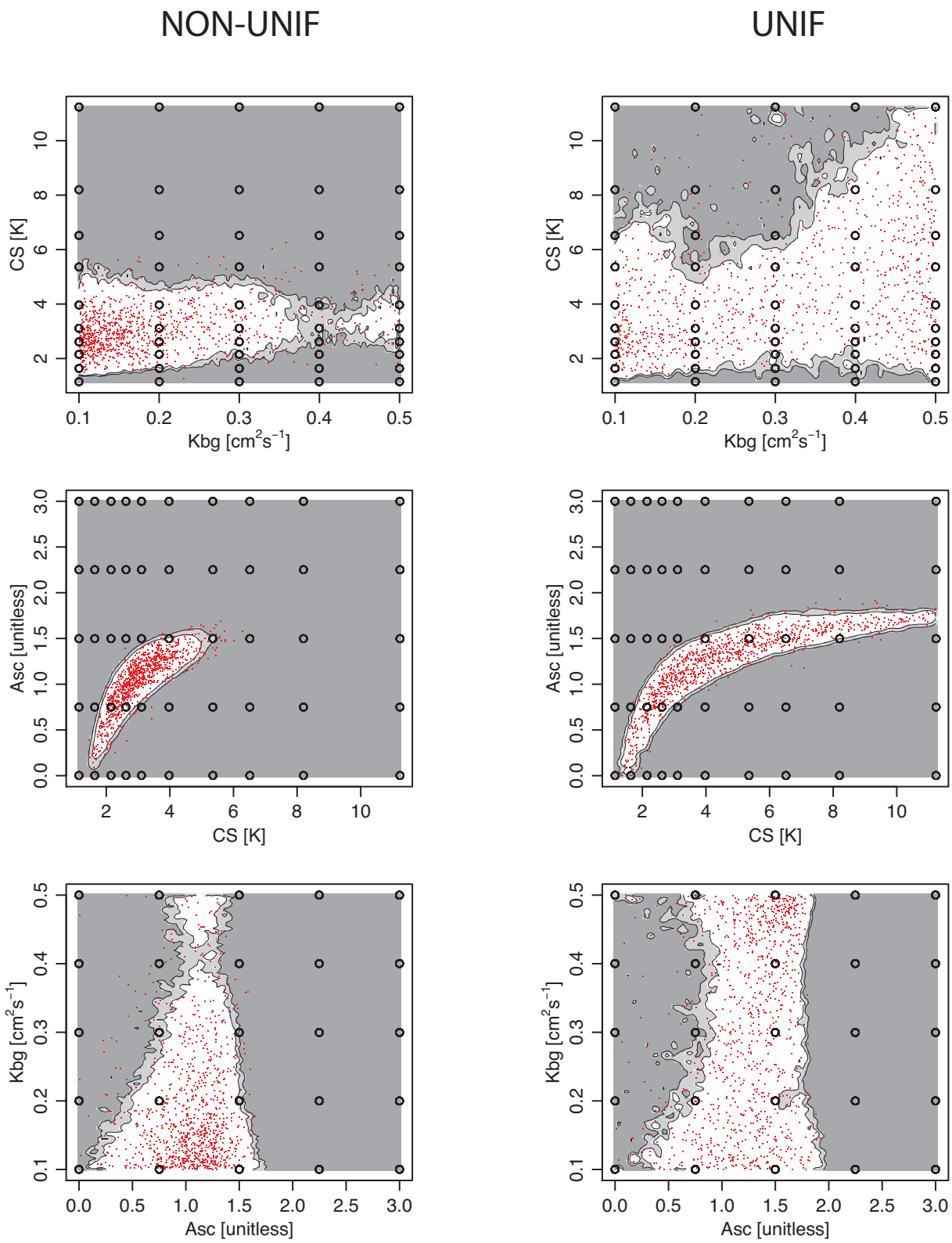

Figure 4: Bivariate joint pdfs for model parameters. Left: for the NON-UNIF experiment, right: for the UNIF experiment. The contour lines delineate the 90% and 95% posterior credible intervals. A 1000-member thinned MCMC chain is plotted using red dots. Parameters used for the UVic ESCM ensemble are shown in thick black circles.